https://doi.org/10.18321/ectj1077

Study of Icaritin Films by Low-Energy Electron Beam Deposition

Tongfei Cheng[1], Jinxing Cao[1], Xiaohong Jiang[1]*, M.A. Yarmolenko[2], A.A. Rogachev[2], A.V. Rogachev[2]

[1]International Chinese-Belorussian Scientific Laboratory on Vacuum-Plasma Technology, Nanjing University of Science and Technology, 200, Xiaolingwei str., Nanjing 210094, China
[2]Francisk Skorina Gomel State University, 104, Sovetskaya str., Gomel 246019, Belarus

Article info

Received:
1 April 2021

Received in revised form:
16 May 2021

Accepted:
25 June 2021

Keywords:
Low-energy Electron Beam Deposition; Icaritin Film; Material Characterization; Film Release; Biocompatibility

Abstract

In this paper, icaritin film was prepared by low-energy beam electron beam deposition (EBD). The material test showed that the structure and composition of icaritin were not changed after electron beam deposition. Then, the film was sliced and immersed in simulated body fluids, it can be seen that the film was released quickly in the first 7 days. With the extension of soaking time, the release rate gradually slowed down, and the release amount exceeded 90% in about 20 days. In vitro cytotoxicity test showed that the relative cell viability rate of the film was still 92.32±1.30% ($p<0.05$), indicating that the film possessed excellent cytocompatibility.

1. Introduction

Metal-based implant materials have excellent mechanical properties, machinability and favorable stability, which are often used in bone tissue engineering to repair or replace human bone tissue [1], accounting for about 70–80% of the total implant materials [2]. Among them, titanium and titanium alloy material has good biocompatibility and osseointegration [3–4], corrosion resistance, excellent mechanical properties, low density, high strength, the modulus of elasticity is closest to human bone, high tensile strength, yield strength and fatigue strength, etc. [2, 5–9], and they are now widely used implants medical metal materials.

However, these implants themselves lack the ability to form or induce osteogenesis. Before implant implantation, loading these medical metal materials for bone tissue engineering with highly effective bioactive factors can promote tissue healing, bone remodeling and bone repair around the scaffold [10]. Catherine D. Reyes et al. coated the surface of the implant with bioactive factors, and compared with the unmodified implant, the coating effectively improved the bone formation and repair around the implant [11]. Jeroen J.J.P. van den Beucken et al. prepared DNA coating on titanium substrate using electrostatic self-assembly technology, and the results showed that compared with the uncoated control group, the coating effectively increased the proliferation of primary rat dermal fibroblasts [12]. These studies have proved that the loading of bioactive factors on the surface of implants has positive effects on tissue healing and bone repair. In order to make the implant have better osteointegration ability, it is also important to promote the accumulation ability of osteoblasts on the surface of the implant. Some studies have also enhanced the cell adhesion ability by covering the surface of the titanium substrate. Dan-li Fu et al. synthesized the nanostructured HA and Sr-HA coatings by electrochemical method on the surface of a titanium substrate, and the Sr-HA coating evidently enhanced the adhesion of rat MSCs [13]. Min-Chul Kim et al. applied the Avidin-Biotin Binding System to the surface of the scaffold to promote cell adhesion [14].

*Corresponding author.
E-mail: jiangxh24@njust.edu.cn

© 2021 Eurasian Chemico-Technological Journal.
This is an open access article under the CC BY license (http://creativecommons.org/licenses/by/4.0/).

Bone marrow stromal cells (BMSCs), a type of stem cells located in bone marrow [15], have the potential to differentiate into osteoblasts and adipocytes [16], and which are the most popular seed cells for bone tissue engineering. A balance of osteoblastic and adipocyte differentiation is key to maintaining skeletal integrity and bone homeostasis [17]. Imbalanced bone formation, reduced bone formation, accompanied by increased bone marrow fat formation, which can lead to osteoporosis and necrosis of the femoral head [18–21]. Bone morphogenetic protein (BMP) is a growth factor that promotes bone formation activity and can induce bone marrow stromal cells to differentiate into osteoblasts [22]. As one of the effective active components of Epimedium, a traditional Chinese medicine commonly used in orthopedics and traumatology, icaritin (ICA) can promote the differentiation of bone marrow stromal cells into osteoblasts by up-regulating the expression of the bone morphogenetic protein, and also inhibit the differentiation of bone marrow stromal cells into other cells, such as adipocytes or skeletal muscle cells [23–25]. Herein, icaritin has become an effective drug for the prevention and treatment of femoral head necrosis and osteoporosis [26–29]. Traditional Chinese medicine Epimedium has a long history in the treatment and prevention of a variety of orthopedic diseases. Epimedium, one of its effective components, was able to enhance the differentiation and proliferation of osteoblasts, has a variety of biological activities and pharmacological effects, and has a good value in clinical application [30–31].

At present, icaritin is mostly used orally or by irrigation, which requires long-term use to work. The application of icaritin to the affected area on the surface of the scaffold with coating loading is still lacking. In this study, we attempted to deposit icaritin films on the substrate surface by low-energy electron beam deposition, and to explore the novel application direction of icaritin in bone tissue engineering. Our group has successfully prepared a variety of bioactive films by EBD method, which has a certain theoretical support and experimental basis for the subsequent research on the prolonged release and degradation of film. Icaritin has a variety of pharmacological effects and high activity towards cardiovascular, immune system, bone metabolism and sexual function, and has been widely used in clinical practice. However, its shortcomings such as poor water solubility and low oral bioavailability limit its clinical application. This study aimed to deposit icaritin film on the surface of the implant by EBD method, so that the biologically active icaritin could directly act on the target site, this may help solve the problem of low oral bioavailability.

2. Materials and methods

2.1. Materials

Icaritin was purchased from Yuanye Biotechnology Co., Ltd (Shanghai, China). Ti sheet (100±10 μm) was provided by Qianchui Metal Products Co., Ltd (Wuxi, China), single crystal silicon wafer (500±10 μm) was supplied by Ruicai Semiconductor Co., Ltd (Suzhou, China), KBr salt tablets (1000±10 μm) was obtained from Botianshengda Co., Ltd (Tianjin, China), MC3T3-E1 cells were purchased from the Chinese Academy of Sciences Shanghai Cell Bank, PBS (CNM20012) was purchased from Wuhan Boster Biological Technology (Wuhan China), Dimethyl Sulfoxide-d6 was supplied by Energy Chemical (Shanghai, China).

In this paper, titanium wafer, silicon wafer, KBr salt wafer as the substrate. Titanium sheet, silicon sheet as the substrate before use, after repeated ultrasonic cleaning with anhydrous ethanol and deionized water, drying in 70 °C oven for reserve, KBr salt sheet can be directly used in the coating. Pure Ti foil is selected as the substrate because of its non-toxic and good biocompatibility characteristics. Besides, compared with alloys, its composition is simple which is easy to characterize and analyze in subsequent research.

2.2. The coating deposition technique

The low-energy electron beam deposition equipment used in this paper is independently developed by the Chinese-Belarusian Scientific laboratory on Vacuum-Plasma Technology. The coating was deposition by means of vacuum continuous exposure of a low-energy electron beam on the target. In the deposition process, the operating current and voltage parameters fluctuate in a specific range: Accelerating Voltage = 0.68±0.1 kV, Cathode Current = 6.6±0.1A. If the current and voltage are too low. The target material cannot be excited. If the current and voltage are too high, it may lead to sputtering of the target material and uneven film deposition. Under the condition of a high vacuum, the tungsten filament in the electron gun is heated and then emits hot electrons. The hot electrons are accelerated to gain kinetic energy and bombarded

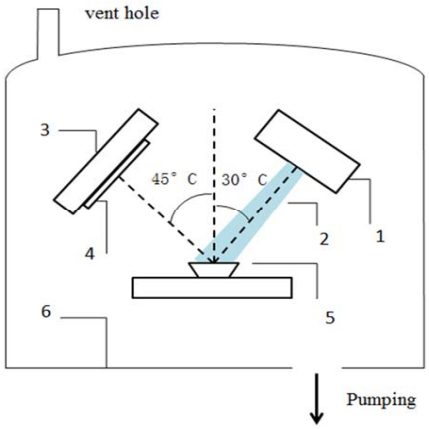

Fig. 1. Schematic diagram of EBD deposition principle: 1 – electron gun; 2 – electron beam; 3 – substrate support; 4 – substrate; 5 – target material; 6 – vacuum chamber.

to the target material. The target material converts the kinetic energy into heat energy and gasifies it to form an active gas phase, which is deposited on the substrate at last [32–33]. The power of the electron beam can be adjusted and the evaporation rate of the target material can be controlled by adjusting the working current and voltage of the electron beam. The schematic diagram of film deposition by EBD method is shown in Fig. 1. It should be noted that the whole process is carried out in the chamber with a high vacuum (5×10^{-4} Pa) whose temperature depends on the room temperature (25 °C in normal) and the temperature of the electron beam area depends on the values of voltage and current.

Compared with the traditional method of preparation of thin film materials, EBD method in the preparation of thin films can be a step in the process of synthesis, solvent-free, and avoid contamination by impurities in the environment [34], the adhesion between the prepared film and the substrate is strong, EBD prepared film also has features of thickness control and good repeatability, conducive to industrial production applications [35].

2.2. Characterization

2.2.1. Composition and structure of films

In this paper, the structure of icaritin film and powder was analyzed by liquid nuclear magnetic resonance spectrometer (Bruker AVANCE III 500 MHz), Deuterium dimethyl sulfoxide was used as deuterium reagent. Fourier transformed infrared spectrometer (Bruker Vertex-70) was used to study the molecular structure of thin films deposited on KBr salt sheets. The scanning range was 4000–300 cm^{-1}, and the resolution was 4 cm^{-1}. The elemental composition of the composite film was qualitatively analyzed by X-ray photoelectron spectroscopy (Phi QUANTERA II). Al Kα was used as the X-ray source (Hν =1486.6eV). The spot size was 200×250 μm^2.

2.2.2. Analysis of film surface properties

The Contact Angle Meter (FCA2000A2, Shanghai AFES Precision Instrument Co., Ltd) is used in this paper. The contact angle measuring range is 0°–180°. Contact Angle display accuracy: ±0.01°; Contact Angle measurement accuracy: ±0.1°. Surface morphology and roughness of a composite membrane were measured using Dimension Icon-type AFM (Bruker AXS). The scanning area was 5×5 μm, Tapping the sample surface in Tapping mode. Finally, the surface roughness of the membrane was assessed using root roughness (RQ).

2.2.3. Morphological characterization

SEM (FEI Quanta 250FEG) was used to observe the surface morphology of the film. Since the sample is not conductive film, the sample must be sprayed with gold before testing to improve its conductivity, so as to obtain a high-definition image. Spray gold using a gold spray instrument (Quorum Technologies Ltd).

2.2.4. Release characteristics of thin films

In this paper, the sample of icaritin film was studied and tested by UV-Vis spectrophotometer (Thermo Fisher EVOLUTION220). The wavelength range was 190~1100 nm. The maximum absorption peak of Icaritin was 225 nm.

2.2.5. Cytotoxicity test

MTT assay was used to detect the cell viability changes of MC3T3-E1 cells after 168 h co-culture with the sample. MC3T3-E1 cells in the logarithmic growth phase were taken for cell count; cell concentration was adjusted and inoculated into 24-well plate according to 1×10^4 cells/well. The cells were cultured overnight in a constant temperature incubator at 37 °C and 5% CO_2 to make the cells adherent. According to the group treatment above, the culture time was 168 h. Remove the culture medium containing the sample. The Wells were

cleaned three times with PBS and cultured in an incubator at 37 °C for 4 h with 500 μL medium containing 0.5 mg/mL MTT, 5% CO_2. The medium in the pore was carefully absorbed, 600 μL DMSO was added, and placed in a shaker at room temperature and low speed for 10 min to fully dissolve the crystals. The absorbance at 570 nm was measured with a full-wavelength microplate instrument.

Cytotoxicity and cell viability were calculated as follows:

Cytotoxicity = $[(OD_{Control}-OD_{Treated})/OD_{Control}] \times 100$

Cell viability = $(OD_{Treated}/OD_{Control}) \times 100$

$OD_{Control}$ = Optical density of control and $OD_{Treated}$ = optical density of composite films. Cell viability greater than 75% can be considered non-cytotoxic [36].

3. Results and discussion

3.1. ^{1}HNMR

The ^{1}HNMR spectra of icaritin film and icaritin powder prepared by EBD method were compared and analyzed. To evaluate the effect of EBD on the molecular structure of icaritin.

The ^{1}HNMR liquid NMR spectra of icaritin powder and icaritin film prepared by EBD method are shown in Fig. 2. The ^{1}HNMR spectra of icaritin powder can be roughly divided into aliphatic region (δ = 1–6.5 ppm) and aromatic region (δ = 7–13 ppm). The ^{1}HNMR spectra of icaritin powder were analyzed based on chemical shift: 12.30 ppm and 10.59 ppm were Ar-OH. The peak values at 9.45, 8.17 and 7.05 ppm were AR-H. 6.25 ppm is R-OH. 3.80 ppm is the signal of -O-CH_3. The signal of -CH_2 was at 2.76 ppm and 1.53 ppm. The peak of –R-CH_3 was found at 1.15 ppm. The ^{1}HNMR spectra of icaritin thin films and icaritin powder were corresponding to each other by low power electron beam evaporation deposition. The characteristic peaks contain all kind of hydrogen atoms in icaritin film without chemical shifts. Meanwhile, there are no redundant peaks, which indicated that the composition and structure of icaritin were not changed after the evaporation deposition of icaritin by the electron beam.

3.2. FT-IR

In the FTIR spectrum of icaritin powder (Fig. 3(2)), the special absorption peak of the ketone hydroxyl group was found at 1650.84 cm^{-1}. The 1599.15 cm^{-1} region is the absorption peak of the aromatic ring. The absorption peaks of aromatic ethers were at 1309.08 cm^{-1} and 1075–1020 cm^{-1}. The coupling of C-O stretching vibration is observed at 1300 cm^{-1}. The bending vibration of the phenolic hydroxyl group is at 1251.64 cm^{-1}. The characteristic absorption peak of the hydroxyl group in tertiary alcohol was 1156.86 cm^{-1}. The peak at 3468.81 cm^{-1} and 3299.36 cm^{-1} is the O-H stretching vibration. The stretching vibration of C-H is observed at 2966.21 cm^{-1}. Generally, the place where the hydroxyl absorption peak is high in frequency (greater than 3000 cm^{-1}), so the absorption peak greater than 3000 cm^{-1} usually indicates the presence of hydroxyl in the molecule.

In the FTIR spectra of icaritin film (Fig. 3(1)), the absorption peak of the ketone hydroxyl group was 1653.30 cm^{-1}. The region of aromatic ring

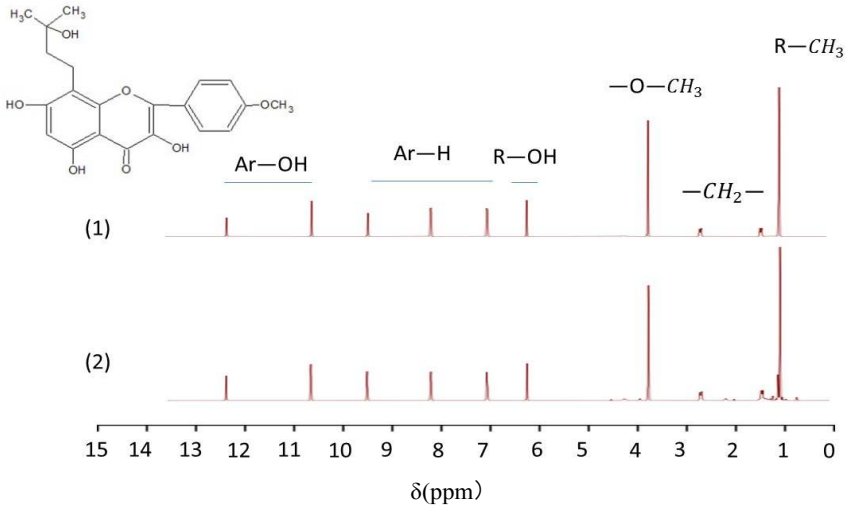

Fig. 2. ^{1}HNMR of icaritin powder and icaritin film: 1 – icaritin powder; 2 – icaritin film.

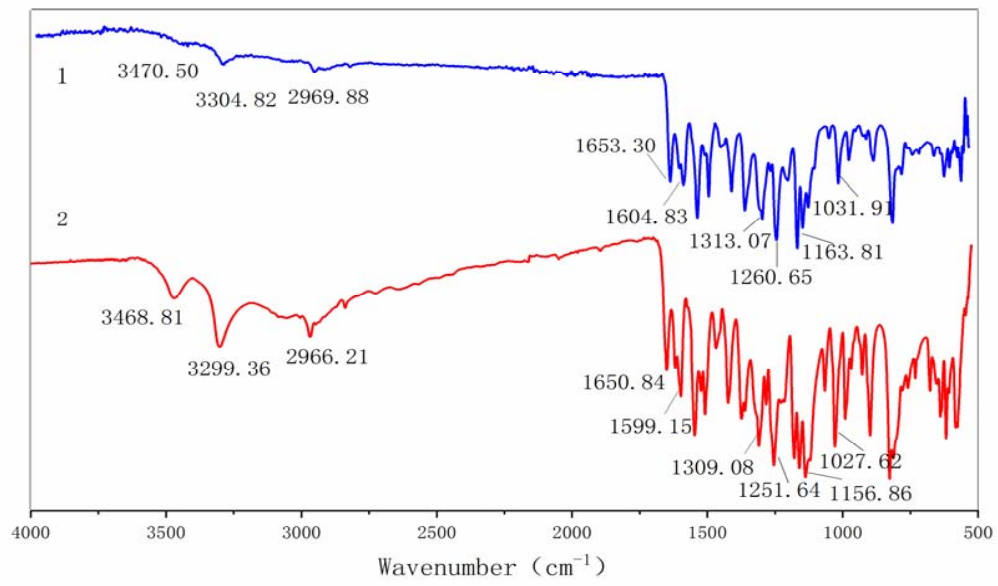

Fig. 3. Infrared spectra of icaritin powder and icaritin film: 1 – icaritin film; 2 – icaritin powder.

absorption peak was 1604.83 cm^{-1}. The bending vibration of the phenolic hydroxyl group is at 1260.65 cm^{-1}. The characteristic absorption peak of the hydroxyl group of tertiary alcohol is at 1163.81 cm^{-1}. The stretching vibrations of O-H are evident at 3470.50 cm^{-1} and 3304.82 cm^{-1}. The stretching vibration of C-H is observed at 2969.88 cm^{-1}.

Through the above analysis and comparison, it is shown that the FTIR spectra of icaritin powder and icaritin film are the same, and the special functional groups of icaritin can be found in the FTIR spectra, which further verifies that the characteristic functional groups of icaritin are not destroyed after the evaporation deposition of icaritin into film by EBD method, which agrees well with the ^{1}HNMR results.

3.3. XPS

Figure 4 shows the results of XPS analysis of icaritin powder and icaritin film prepared by EBD method. According to the full spectrum (Fig. 4. A-1, A-2), both icaritin powder and icaritin film contain C and O elements, where the proportions of C and O are 84.8%, 15.2% and 87.5%, 12.5% respectively. According to the C1s spectrum of icaritin powder (Fig. 4. B-1), The composite peak of C1s can be fitted to three characteristic peaks, which correspond to the C-C bond of the aliphatic group at 284.76 eV, 286.37 eV should correspond to C-O bond, 288.81 eV corresponds to the C=O bond. The peak areas account for 68.78%, 22.78% and 8.44% respectively. According to the C1s spectrum of icaritin film (Fig. 4. B-2), The composite peak of C1s can be fitted to three characteristic peaks, which correspond to the C-C bond of aliphatic group at 284.79 eV, 286.38 eV should correspond to C-O bond, 288.62 eV corresponds to the C=O bond. The peak areas account for 77.41%, 20.65% and 1.94% respectively. In the O1s spectrum of icaritin powder and icaritin film (Fig. 4. C-1, C-2), O element merged into one peak at 532.50 and 532.77, respectively. Compared with the full spectrum of icaritin powder and icaritin film, the content of elements is the same. The position and shape of the three characteristic peaks of C1s are the same, and the characteristic peaks obtained by fitting can also correspond to the structure of icaritin itself.

Figure 5 shows the XPS analysis results after icaritin immersion in simulated body fluids for 7 days and 21 days. According to the C1s spectrum of icaritin film for 7 days (Fig. 5. E-1), The composite peak of C1s also can be fitted to three characteristic peaks, which correspond to the C-C bond of the aliphatic group at 284.86 eV, 286.60 eV should correspond to C-O bond, 288.58 eV corresponds to the C=O bond. The peak areas account for 71.93%, 22.75% and 5.32% respectively. According to the C1s spectrum of icaritin film for 21 days (Fig. 5. E-2). The composite peak of C1s also can be fitted to three characteristic peaks, which correspond to the C-C bond of aliphatic group at 284.79 eV, 286.37 eV should correspond to C-O bond, 288.51 eV corresponds to the C=O bond. The peak areas account for 68.14%, 23.87% and

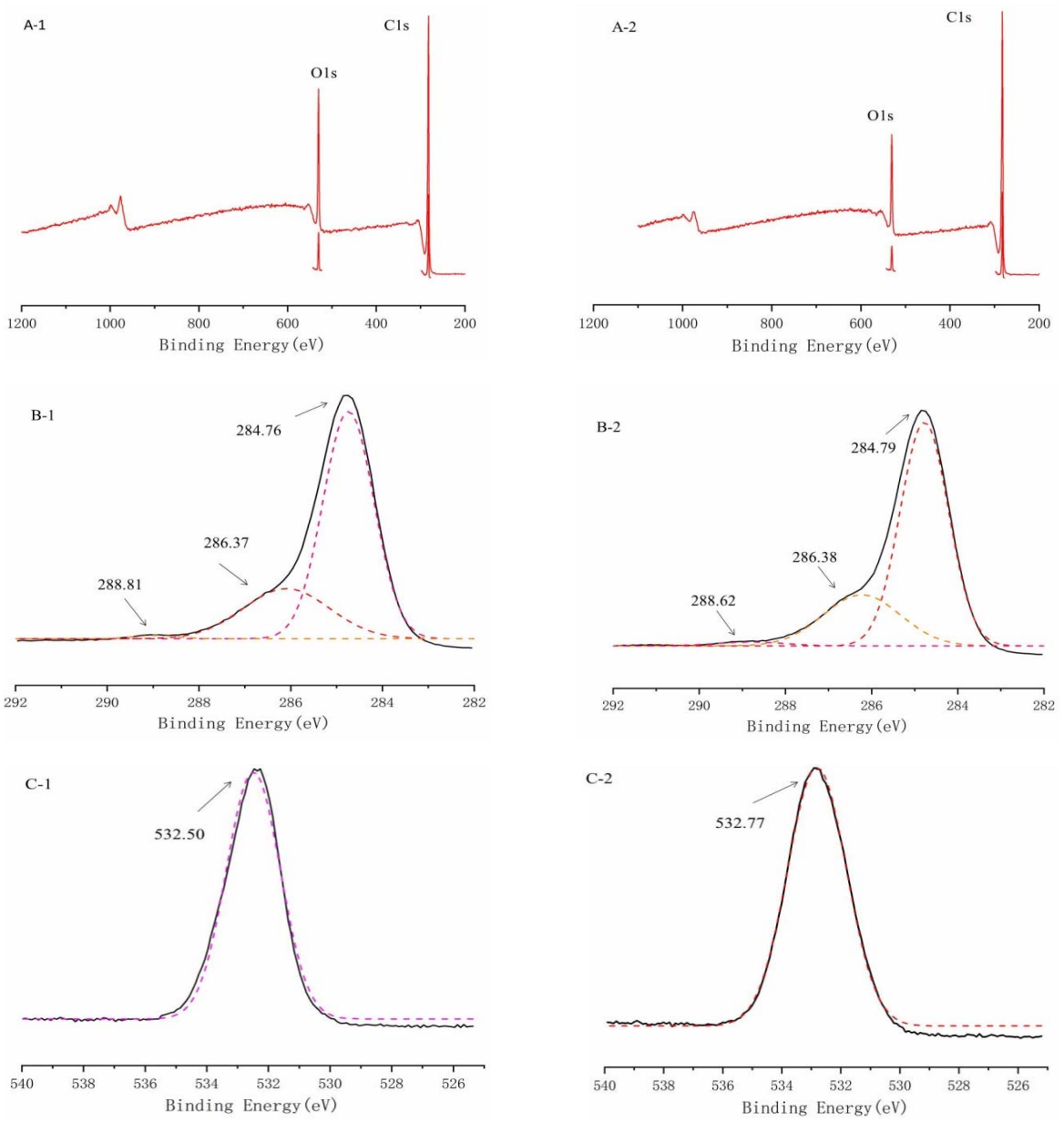

Fig. 4. XPS spectra: A – full spectrum; B – C1s spectra; C – O1s spectra 1 – Icaritin powder; 2 – Icaritin film.

7.99% respectively. In the O1s spectrum of icaritin film for 7 days and 21 days (Fig. 5. F-1, F-2), O element merged into one peak at 532.56 and 532.47, respectively. The results showed that icaritin still existed on the substrate surface after 7 days and 21 days immersion of simulated body fluids, and the characteristic peaks obtained by C1s fitting were the same as those obtained before immersion, which proved that the composition and structure of icaritin film could remain stable after immersion of simulated body fluids.

3.4. The contact angle

Figure 6B shows the contact angle test diagram of icaritin film. The molecular formula of icaritin contains both hydrophobic group -CH_3 and hydrophilic group -OH. The measured results show that the contact angle of pure icaritin film is 81.3°, and the contact angle is less than 90°. By contrast, the contact angle of the titanium substrate surface is 104.5° (Fig. 6A), which belongs to the hydrophobic surface. The deposition of icaritin film improves the wettability of the titanium substrate surface. The wettability of the titanium implant surface will affect the cell adhesion of the implant at the early stage of implantation. Considering the interaction between body fluids, cells and tissues and the implant surface, the hydrophilic surface is more suitable than the hydrophobic surface [37–40]. Therefore, the results indicate that the deposition of icaritin film can improve the surface properties of titanium substrate.

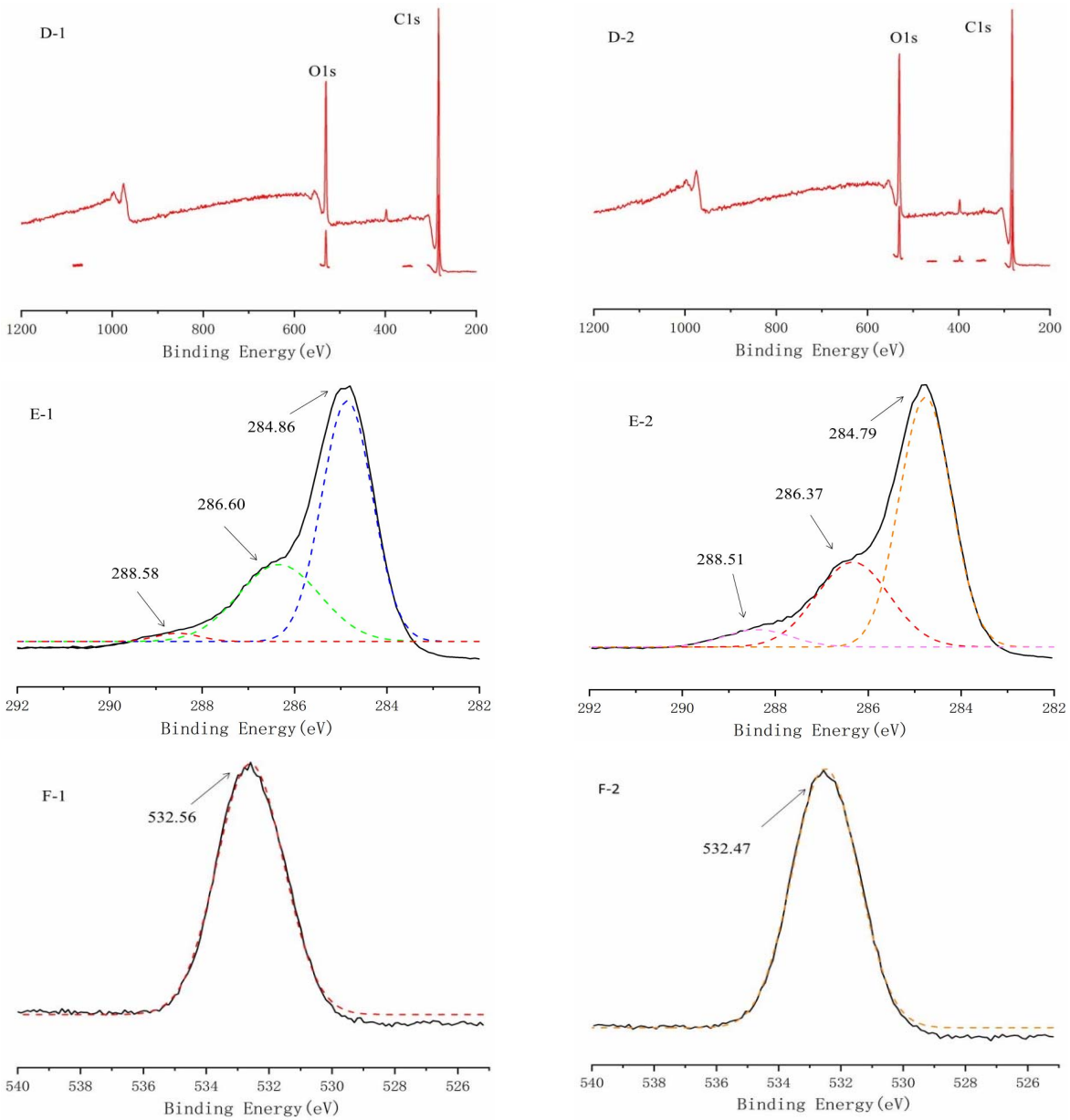

Fig. 5. XPS spectra: D – full spectrum; E – C1s spectra; F – O1s spectra 1 – Icaritin film for 7 days; 2 – Icaritin film 21 days.

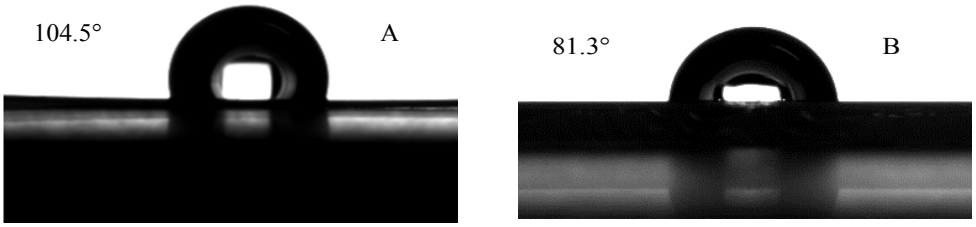

Fig. 6. The Contact Angle Test: A – titanium substrate; B – Icaritin film.

3.5. AFM

Figure 7B is the AFM diagram of icaritin film; the substrate used for deposition was Si sheet (Fig. 7A). The AFM shows that the surface of the film is flat without large particles on the surface. The root means square roughness R_q of the film is 0.348 nm. The corresponding base has an R_q of 0.166 nm. Even though the value of R_q has increased, the R_q of the film is still at a low value. The low roughness indicates that the icaritin film prepared by the EBD method has uniform distribution and a smooth surface.

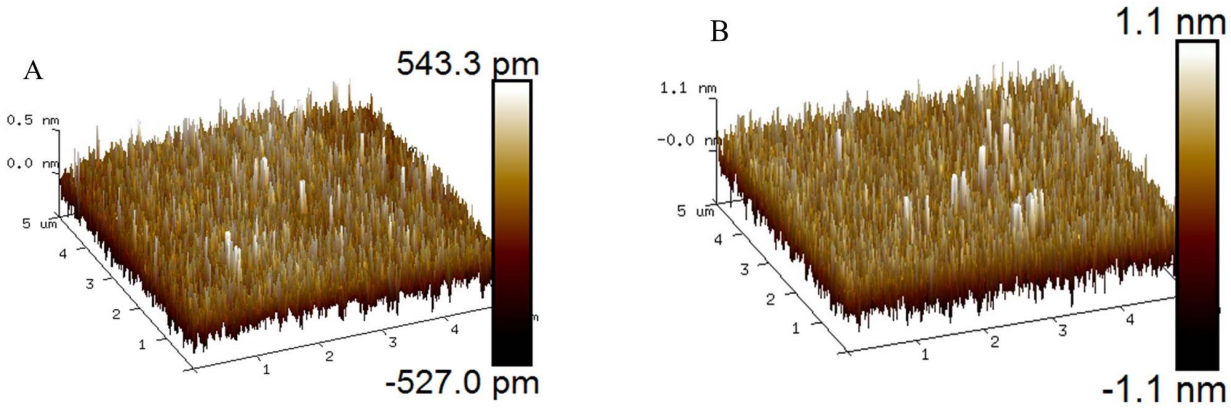

Fig. 7. AFM diagram of icaritin film: A – Si substrate; B – icaritin film.

However, the limitation of AFM is that its probe detection can only observe the morphology and roughness of a very small area on the surface of the sample, and other detection means are needed to prove the overall morphology.

3.6. Surface morphology and thickness

Figure 8A, B shows the surface morphology of the icaritin film based on titanium at different magnifications. It can be seen that the surface of icariin film is flat. Larger debris and smaller debris are present in some areas. In the deposition process, icariin powder is firstly evaporated into an active gas phase component under the impact of the electron beam and then deposited on the substrate surface to form thin films. Therefore, the energy used by the electron beam evaporation is very important. Slightly higher electron beam energy will make the gas phase components too active and form gas phase components crosslink, and then this may lead to uneven deposition.

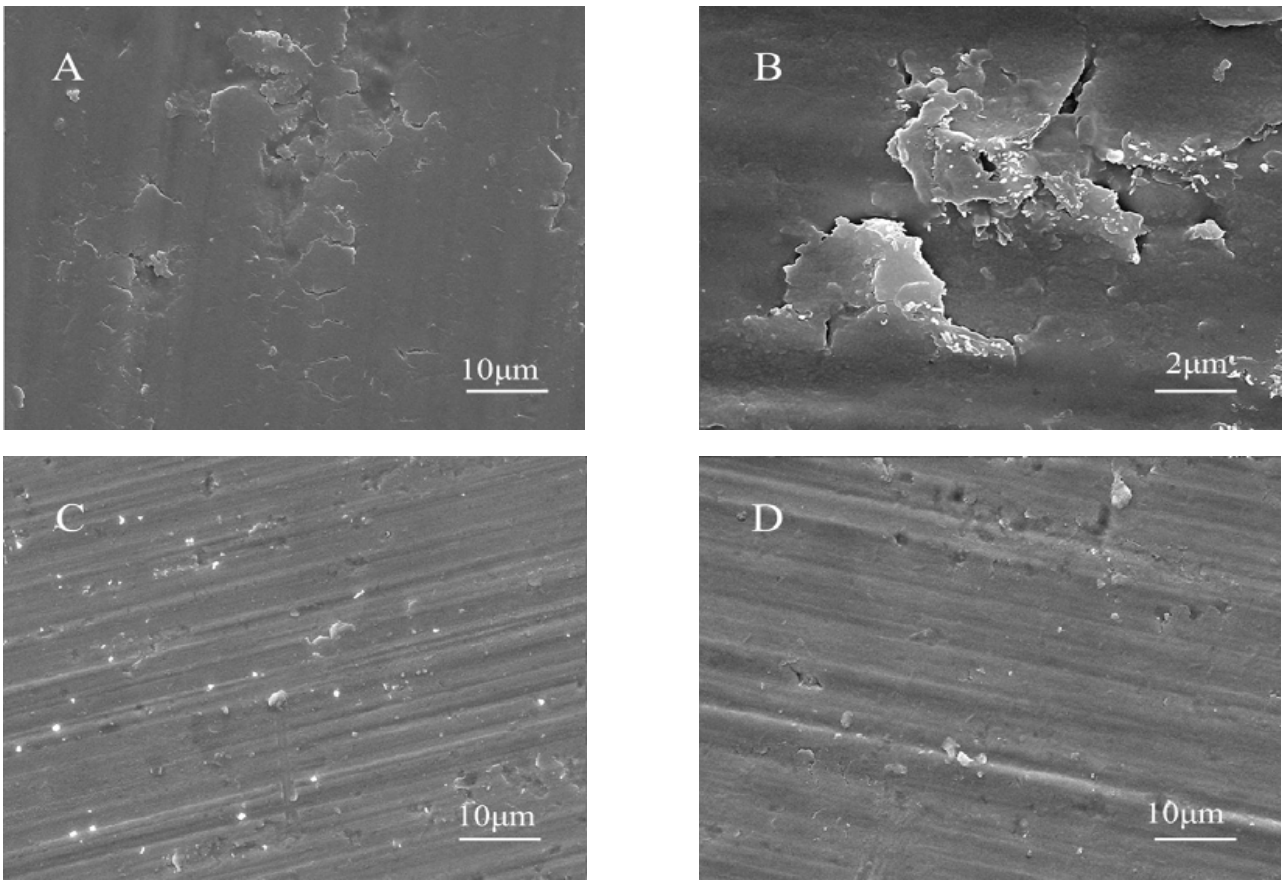

Fig. 8. SEM of icaritin film (A, B – icaritin film at different magnification; C – icaritin film for 7 days; D – icaritin film for 21 days).

Figure 8 C, D shows the surface morphology of the icaritin film after immersion in simulated body fluids for 7 days and 21 days. As can be seen from the result, after 7 days of the film release, part of the titanium substrate was exposed, a large amount of film was released, and small particles of icaritin were unevenly distributed on the surface, 21 days after film release, the film is completely released, and only a small part of icariin fragments remain.

We can learn from the results: the release of icaritin film in prophase is fast, most of the icaritin is released in about 7 days so that we can see that the titanium base is bare. From 7 days to 21 days of the process, the release of icaritin film is almost completely. The result is consistent with our release curve test results.

3.7. The release curve

To study the release kinetics of icaritin, a film with a diameter of 5 mm was soaked in 20 ml of simulated body fluids and stored in a thermostatic shaker at a temperature of 30 °C. The absorbance of the solution was measured by UV-Vis spectrophotometer, and the release curve of icaritin was obtained. From the release curve of icaritin film (Fig. 9), it can be seen that the release of icaritin is faster in the 7 days before soaking, and the release rate slows down gradually with the increase of immersion time, and releases more than 90% in 20 days or so, and the release curve tends to flatten out around 30 days. The results showed that the release period of icaritin film could be about one month even if it acted directly with the simulated body fluids, which ensured its long-term effect.

Xue Peng et al. used 3D printing technology to prepare β-tricalcium phosphate as the scaffold loaded with icaritin. The results showed that the release of icaritin became slow around 16 days and was complete around 30 days [41].

3.8. Cytotoxicity test results

As a film loaded on the surface of the implant, it should have excellent biocompatibility. Figure 10 shows the cell viability of MC3T3-E1 cells on the icaritin film after 168 h. The cell viability of icaritin film is about 92.32%. According to the toxicity rating of the United States Pharmacopoeia, according to the mean value of RGR, the value-added rates corresponding to toxicity grades 0, 1, 2, 3, and 4 were 100%, 80%–90%, 50%–79%, 30%–49%, and 0–29%. Our film has a toxicity rating of level 1.

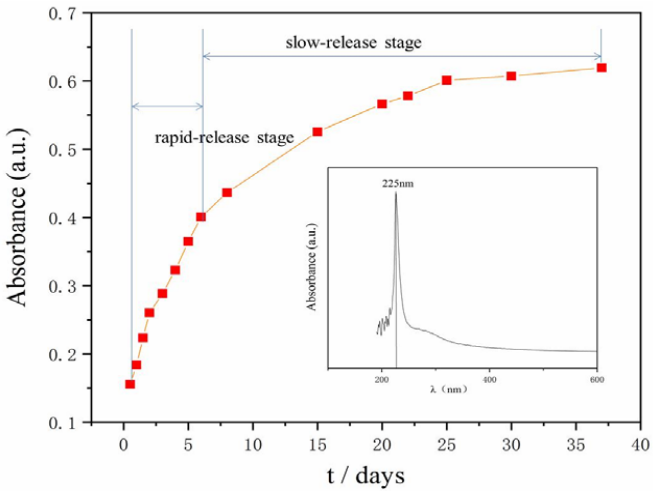

Fig. 9. Release curve of icaritin film.

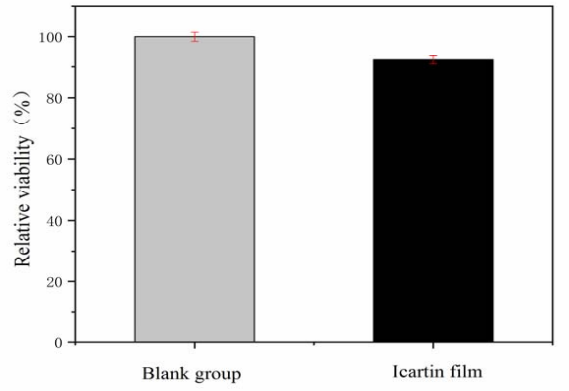

Fig. 10. Cytotoxicity test results.

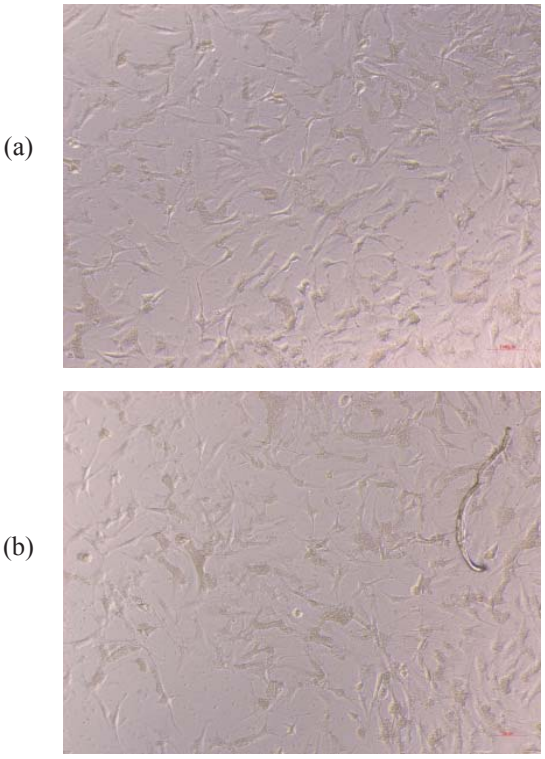

Fig. 11. Picture of cytotoxicity test: (a) – Blank control group; (b) – Icaritin film.

This proved that the film was non-cytotoxic. Furthermore, after culturing with MC3T3-E1 cells for 168 h, the cell morphology on the surface of the icaritin film was observed. As can be seen in Fig. 11, the MC3T3-E1 cells on the surface of the film maintained their normal fibroblast phenotype and healthy spindle-like shape. Overall, the icaritin film possessed good cytocompatibility.

4. Conclusions

In this study, icaritin film was deposited on the substrate surface by the low-energy electron beam evaporation method. The NMR, FTIR, XPS tests proved that the composition and structure of icaritin did not change after the deposition by electron beam evaporation, which ensured the feasibility of application. The test results of the contact angle indicate that the deposition of icaritin film improves the wettability of the titanium substrate surface. From the release curve of icaritin, it can be seen that the release of icaritin is faster in the 7 days before soaking, and the release rate slows down gradually with the increase of immersion time, and releases more than 90% in 20 days or so. Finally, the cell viability of the icaritin film has good biocompatibility. Based on the above results, this work can provide a facile path to obtain the bioactive film, which can be a promising application direction of icaritin in bone tissue engineering.

Acknowledgement

This work was supported by the Intergovernmental Cooperation Projects in the National Key Research and Development Plan of the Ministry of Science and Technology of the People's Republic of China (No. 2016YFE0111800), and Nanjing University of Science & Technology Independent Research Project (No. 30919013301).

References

[1]. P. Chocholata, V. Kulda, V. Babuska, *Materials* 12 (2019) 568. DOI: 10.3390/ma12040568

[2]. M. Niinomi, M. Nakai, J. Hieda, *Acta Biomat.* 8 (2012) 3888–3903. DOI: 10.1016/j.actbio.2012.06.037

[3]. S.M. Perren, P. Regazzoni, A.A. Fernandez, *Acta Chir. Orthop. Traumatol. Cech.* 84 (2017) 85–90. PMID: 28809623

[4]. S.W. Fage, J. Muris, S.S. Jakobsen, J.P. Thyssen, *Contact Dermatitis* 74 (2016) 325–345. DOI: 10.1111/cod.12565

[5]. Zhang Wen-yu, *Metal World* 1 (2020) 21–27 (in Chinese). DOI: 10.3969/j.issn.1000-6826.2020.01.007

[6]. S.M. Perren, P. Regazzoni, A.A. Fernandez, *Acta Chir. Orthop. Traumatol. Cech.* 84 (2017) 9–12. PMID: 28253940

[7]. M. Niinomi, M. Nakai, *Int. J. Biomater.* 2011, ID 836587. DOI: 10.1155/2011/836587

[8]. P. Afzali, R. Ghomashchi, R.H. Oskouei, *Metals* 9 (2019) 878. DOI: 10.3390/met9080878

[9]. S. Xu, G. Zuo, Z. Shuang, Y. Shude, *Shandong Medical Journal* 2019 (30) 107–110 (in Chinese).

[10]. L. Lingrong, L. Yumei, S. Feng, C. Zhenyong, *China Modern Doctor* 23 (2020) 186–192 (in Chinese).

[11]. C.D. Reyes, T.A. Petrie, K.L. Burns, Z. Schwartz, A.J. Garcia, *Biomaterials* 28 (2007) 3228–3235. DOI: 10.1016/j.biomaterials.2007.04.003

[12]. J.J.J.P. van den Beucken, M.R.J. Vos, P.C. Thüne, T. Hayakawa, T. Fukushima, Y. Okahata, X.F. Walboomers, N.A.J.M. Sommerdijk, R.J.M. Nolte, J.A. Jansen, *Biomaterials* 27 (2006) 691–701. DOI: 10.1016/j.biomaterials.2005.06.015

[13]. Dan-li Fu, Qiao-hong Jiang, Fu-ming He, Baiping Fu, *J. Zhejiang Univ. Sci. B* 18 (2017) 778–788. DOI: 10.1631/jzus.B1600517

[14]. Min-Chul Kim, Min-Ho Hong, Byung-Hyun Lee, Heon-Jin Choi, Yeong-Mu Ko, Youn-Keun Lee, *Ann. Biomed. Eng.* 43 (2015) 3004–3014. DOI: 10.1007/s10439-015-1347-y

[15]. P.G. Robey, A.A. Kuznetsov, M. Riminucci, P. Bianco, Bone Marrow Stromal Cell Assays: In Vitro and In Vivo. In: Hilton M. (eds) Skeletal Development and Repair. Methods in Molecular Biology 1130 (2014) 279–293. DOI: 10.1007/978-1-62703-989-5_21

[16]. J.L. Spees, R.H. Lee, C.A. Gregory, *Stem Cell Res. Ther.* 7 (2016) 125. DOI: 10.1186/s13287-016-0363-7

[17]. P. Xue, X. Wu, L. Zhou, H. Ma, Y. Wang, Y. Liu, J. Ma, Y. Li. *Biochem. Bioph. Res. Co.* 433 (2013) 226–231. DOI: 10.1016/j.bbrc.2013.02.088

[18]. P. Astudillo, S. Ríos, L. Pastenes, A.M. Pino, J.P. Rodriguez, *J. Cell. Biochem.* 103 (2008) 1054–1065. DOI: 10.1002/jcb.21516

[19]. J. Seamon, T. Keller, J. Saleh, Q. Cui, *Arthritis*, 2012, ID 601763. DOI: 10.1155/2012/601763

[20]. N. Han, Z. Li, Z. Cai,Z. Yan, Y. Hua, C. Xu, *J. Cell Mol. Med.* 20 (2016) 2173–2182. DOI: 10.1111/jcmm.12917

[21]. M.B. Berger, K.B. Bosh, T.W. Jacobs, D.J.

Cohen, Z. Schwartz, B.D. Boyan, *J. Orthop. Res.* 39 (2020) 1908–1920. DOI: 10.1002/jor.24869
[22]. Sheng Hui, Wang Hongfu, *Chinese Journal of Osteoporosis* 1 (2004) 98–102 (in Chinese).
[23]. Liu Xiao Yan. In vivo disposition and metabolic dynamics of icariin. Shandong University, 2009.
[24]. S. Adhikary, D. Choudhary, N. Ahmad, A. Karvande, A. Kumar, V.T.B.M. Pharm, P.R. Mishra, R. Trivedi, *Nutrition* 53 (2018) 64–76. DOI: 10.1016/j.nut.2017.12.003
[25]. Guo Xiaoyu, Ge Baofeng, Chen Keming, Zhen Ping, Zhou Jian, Ma Xiaoni, *Chinese Journal of Osteoporosis* 9 (2013) 897–901 (in Chinese).
[26]. Zeng Hua-ting, Guo Jian, Chen Yan, *Chinese Traditional and Herbal Drugs* 51 (2020) 5372–5380 (in Chinese). DOI: 10.7501/j.issn.0253-2670.2020.20.031
[27]. Hao Zhang, Bailing Wang, Miao Tian, Baohu Lin, Yongheng Zhao, *International Journal of Traditional Chinese Medicine* 6 (2018) 893–896. ID: wpr-693688
[28]. R.Z.L. Lim, L. Li, E.L. Yong, N. Chew, *BBA – Gen. Subjects* 1862 (2018) 1680–1692. DOI: 10.1016/j.bbagen.2018.04.016
[29]. T. Wu, T. Shu, L. Kang, J. Wu, J. Xing, Z. Lu, S. Chen, J. Lv, *Int. J. Mol. Med.* 39 (2017) 984–992. DOI: 10.3892/ijmm.2017.2906
[30]. G. Zhang, L. Qin, H. Sheng, X.-L. Wang, Y.-X. Wang, D. Ka-Wai Yeung, J.F. Griffith, X.-S. Yao, X.-Hui Xie, Z.-R. Li, K.-Man Lee, K.-Sui Leung, *Bone* 44 (2009) 345–356. DOI: 10.1016/j.bone.2008.10.035
[31]. Xin-Hui Xie, Xin-Luan Wang, Ge Zhang, Yi-Xin He, Yang Leng, Ting-Ting Tang, Xiaohua Pan, Ling Qin, *J. Tissue Eng. Regen. Med.* 9 (2015) 961–972. DOI: 10.1002/term.1679
[32]. M. Ramos, E. Fortunati, M. Peltzer, A. Jimenez, J.M. Kenny, M.C. Garrigósa, *Polym. Degrad. Stabil.* 132 (2016) 2–10. DOI: 10.1016/j.polymdegradstab.2016.05.015
[33]. Y. Ramot, M. Haim-Zada, A.J. Domb, A. Nyska, *Adv. Drug Deliver. Rev.* 107 (2016) 153–162. DOI: 10.1016/j.addr.2016.03.012
[34]. Z.Ö. Erdohan, Z. Çam, K.N. Turhan, *J. Food Eng.* 119 (2013) 308–315. DOI: 10.1016/j.jfoodeng.2013.05.043
[35]. P.O. Rujitanaroj, N. Pimpha, P. Supaphol, *Polymer* 49 (2008) 4723–4732. DOI: 10.1016/j.polymer.2008.08.021
[36]. Saral Sarojini K., Indumathi M.P., Rajarajeswari G.R. *Int. J. Biol. Macromol.* 124 (2019) 163–174. DOI: 10.1016/j.ijbiomac.2018.11.195
[37]. R.A. Gittens, L. Scheideler, F. Rupp, S.L.Hyzy, J. Geis-Gerstorfer, Z. Schwartzc, B.D. Boyan, *Acta Biomater.* 10 (2014) 2907–2918. DOI: 10.1016/j.actbio.2014.03.032
[38]. L. Hao, H. Yang, C. Du, X. Fu, N. Zhao, S. Xu, F. Cui, C. Mao, Y. Wang, *J. Mater. Chem. B* 2 (2014) 4794–4801. DOI: 10.1039/C4TB00597J
[39]. C. Zhang, Z. Ding, L. Xie, L.-C. Zhangb, LaizhiWu, Y. Fu, L. Wang, Weijie Lu, *Appl. Surf. Sci.* 423 (2017) 331–339. DOI: 10.1016/j.apsusc.2017.06.141
[40]. R.A. Gittens, R. Olivares-Navarrete, A. Cheng, D.M. Anderson, T. Mc Lachlan, I. Stephan, J. Geis-Gerstorfer, K.H. Sandhage, A.G. Fedorov, F. Rupp, B.D. Boyan, R. Tannenbaum, Z. Schwartz, *Acta Biomater.* 9 (2013) 6228–6277. DOI: 10.1016/j.actbio.2012.12.002
[41]. Xue Peng, Du Bin, Wang Li-ning, Cao Liang-quan, Sun Guang-quan, Liu Xin, Yu Heng-heng, *Chinese Journal of Tissue Engineering Research* 6 (2018) 865–870.